11.3 COMMERCIAL AVIATION ENCOUNTERS WITH SEVERE LOW ALTITUDE TURBULENCE

Paul E. Bieringer†, Brian Martin, Brian Collins and Justin Shaw
MIT Lincoln Laboratory, Lexington, Massachusetts

1. INTRODUCTION*

Turbulence encounters continue to be one of the largest sources of personal injury in both commercial and general aviation. A significant percentage of these encounters occur without warning, at low altitudes, and have been observed to occur outside of the strong reflectivity storm cores where pilots typically anticipate severe wind shear and/or turbulence.

In this paper, statistics illustrating the altitude distributions of specific turbulence encounters are presented. These results suggest that a significant percentage of the moderate and greater turbulence encounters occur at low altitudes. One particularly dangerous form of low altitude turbulence, often associated with convective storms, is the buoyancy wave (BW). Observational evidence of commercial airline encounters with these phenomena indicates that they can cause an impairment of aircraft control that results in significant attitude and altitude fluctuations.

Over the past two years several serious aircraft incidents involving low altitude turbulence have been reported. In our investigation of the meteorological conditions surrounding these incidents, there are strong indications that buoyancy waves played a major role in initiating the turbulence. While encounters with this type of buoyancy wave-induced turbulence can be as severe as microburst wind shear encounters, they are typically not detected by current wind shear detection systems. However, these phenomena do have detectable signatures. We suggest two modifications to existing wind shear detection systems that would make it possible to detect these potentially dangerous phenomena.

2. BACKGROUND

A common misconception regarding aircraft encounters with turbulence is that they primarily occur in the enroute airspace at cruising altitudes (i.e. greater than 18,000 feet agl). This perception may be due in part to the passenger injury statistics that reflect an increase in injuries at cruising altitudes where passengers are more likely to have removed their seat belts to move around the cabin. An analysis of pilot reports (pireps) for the 2002 calendar year over the Corridor Integrated Weather System Domain (Fig. 1) indicates that a significant percentage of the moderate and greater turbulence encounters (over 62 %) occur at or below 18,000 feet (Fig. 2).

While passengers are often belted into their seats at these lower altitudes, the turbulence still poses a safety concern to flight crews working in the cabin, and can affect aircraft control during critical phases of flight. Over the past decade there have been numerous documented commercial aircraft incidents and at least one fatal general aviation accident that have occurred following encounters with low altitude turbulence (Meuse et al. 1996, Miller et al. 1997, Miller 1999, and Bieringer 2002). In nearly all of these documented cases there was evidence that atmospheric buoyancy waves were present at the time and location of the incident.

*This work was sponsored by the Federal Aviation Administration under Air Force Contract No. F19628-00-C-0002. Opinions, interpretations, conclusions, and recommendations are those of the authors and are not necessarily endorsed
by the U.S. Government.

†Corresponding author address: Dr. Paul E. Bieringer, MIT Lincoln Laboratory, 244 Wood Street, Lexington, MA 02420-9108; e-mail: paulb@LL.MIT.EDU

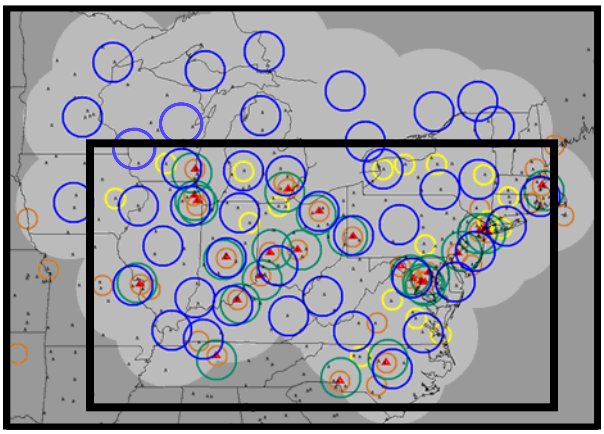

Figure 1. The Corridor Integrated Weather System domain and sensor coverage as of July 2004. The rectangle represents the domain over which the turbulence pilot report statistics were compiled.

Buoyancy waves, often referred to as gravity waves, form in the atmosphere in response to a perturbation of air parcels in a thermodynamically stable environment. The wave-generating perturbations often develop in response to vertical shear of the horizontal wind in the boundary layer. Figure 3 illustrates an idealized thunderstorm outflow encountering vertical shear in the horizontal winds. This is a common scenario during which BW development occurs, but the formation of buoyancy waves is not restricted to the density discontinuities generated by thunderstorm outflows. They can essentially form along any density discontinuity in the atmosphere.

Once the waves have formed, the stable stratification in the lower atmosphere provides a wave-guide along which the energy propagates horizontally. In this situation, atmospheric stability acts as the restoring force since more [less] dense air displaced up [down] tends to return to its original altitude. The resulting oscillations can occur across a relatively broad spectrum of scales ranging from 10's of km to 100's of meters. (A detailed documentation of buoyancy wave observations can be found in Miller et al. 1997, Miller 1999, and Bieringer 2002.) The present study examines buoyancy waves that form at the smaller end of the spectrum.

Much of the physical understanding of buoyancy waves was gained from laboratory fluid dynamics experiments. One such experiment by Simpson (1969) utilized a saline solution and pure water to examine density flows in fluids, which he then related to observations of atmospheric density flows. His study provided physical descriptions and vivid photographs of the turbulence that can form at the boundaries between the fluids. Figure 4 is a photograph of a density current in a transparent tank from Simpson (1969). This phenomenon has been numerically simulated by Droegemeier and Wilhelmson (1987) and Xu et al. (1996). Their studies produced similar waves and demonstrated that the turbulence intensity varies with changes in the vertical environmental shear in the horizontal winds.

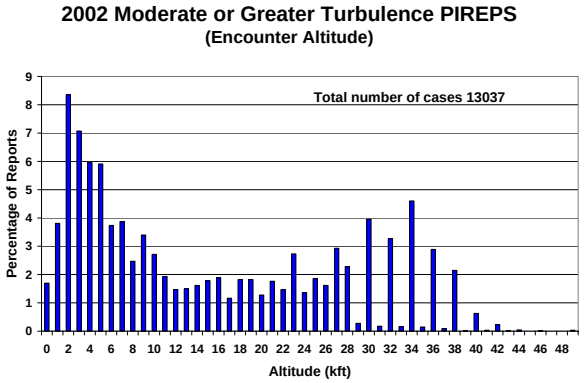

Figure 2. An altitude distribution of turbulence pilot reports over the 2002 calendar year over the Corridor Integrated Weather System domain. The PIREPs data set was provided by the National Center for Atmospheric Research (NCAR).

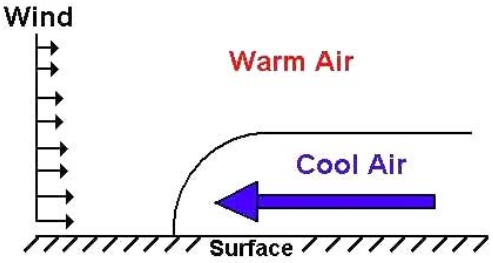

Figure 3. An idealized thunderstorm outflow encountering vertical shear in the environmental winds. (Bieringer, 2002)

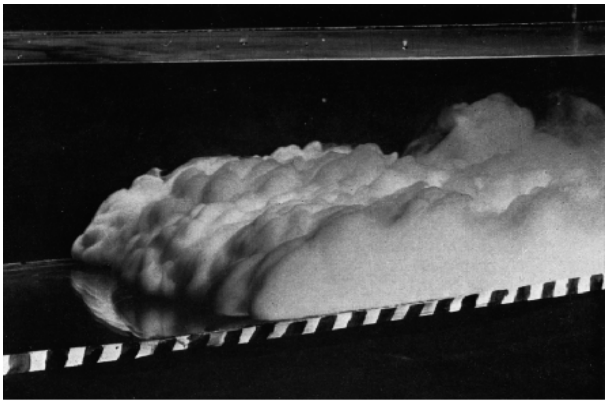

Figure 4. Density current in a transparent tank. The strip at the bottom is marked in intervals of 1 cm. (Simpson, 1969)

3. RECENT BUOYANCY WAVE INCIDENTS

Over the past two years, six additional low altitude buoyancy wave incidents have been brought to the authors' attention through personal contacts in the aviation community. We suspect that most of the aircraft turbulence encounters of this nature go unreported to the aviation weather research community. The following two cases from 2002 are encounters for which the available data permitted extensive and detailed case studies. They illustrate the severity of the hazard posed by low altitude buoyancy wave turbulence.

3.1 DFW Incident: 30 April 2002

On 30 April 2002 the atmosphere in Dallas/Ft Worth was conditionally unstable, supporting the development of isolated severe thunderstorms over the western portion of terminal airspace. Light rain was being reported over the approach paths and runways of the Dallas Ft. Worth International (DFW) Airport when an MD-80 was on final approach to runway 18R. Due to a previous report of moderate-severe turbulence at 3000 feet MSL north of the airport, the pilot requested a runway change. Per request, the MD-80 was switched to runway 17C and cleared for landing.

On their approach to 17C the MD-80 encountered severe turbulence that was described by the pilots as causing significant accelerations followed by losses in airspeed and altitude. The encounter occurred below 3000 feet. While there were other reports of turbulence on this day, this extreme turbulence encounter occurred well outside of any thunderstorm, in weather typically considered to be benign.

On this day the turbulent regions formed along the upper surface of the convective outflows, which created a thermodynamically stable layer conducive to BW development. Surface observations at the time of the incident also indicated that a weak surface boundary was located over the terminal area oriented northwest to southeast. A horizontal shearing of the wind was associated with this boundary; winds north of the boundary were east-southeasterly and south of the boundary were more southeasterly.

The radar data from the DFW and Dallas-Love Field (DAL) Terminal Doppler Weather Radars (TDWRs) indicated that at least two sets of buoyancy waves developed in the wake of dissipating thunderstorms in the region. One set of waves was close to the surface traveling southeastward (likely along the weak surface boundary), and the other set occurred at a higher altitude (~1700 ft) and moved across the area east-northeastward.

The near-surface BWs developed in response to a vertical shear in the horizontal winds observed in the 00 UTC Fort Worth sounding. These waves impacted the northern portions of DFW, and generated wind shear alerts on the Low Level Wind Shear Alert System (LLWAS-NE) 10 minutes before the incident. The higher-altitude set of buoyancy waves crossed over the western portion of DFW and resulted in a wind direction change following their passage 18 minutes prior to the incident. The incident occurred when the two sets of waves intersected over the approach path several miles north of DFW. Doppler weather radar data depicting the intersecting waves and aircraft flight track through the severe turbulence is shown in Figure 5.

3.2 JFK Incident: 29 April 2002

On 29 April 2002, a Boeing 767 encountered significant wind shear and turbulence on approach to runway 13L at JFK. A previous commercial jet also experienced turbulence along this path, prompting the 767 to make a tighter than usual turn on its approach. During the turn, the jet dropped from 1500 to 400 ft before the crew was able to recover and execute a missed approach. No ground-based wind shear detection warnings were issued for this encounter.

At the time of the incident, a warm front was present just south of New York City with a cold front to the west, and a pre-frontal trough extending over the city. The Brookhaven, Long Island (OKX) sounding indicated that the lower atmosphere near the time of the event was stable below an inversion at 4000 ft. The strongest convection associated with this event tracked to the north of the city and was greater than 50 dBZ; however, most of the precipitation directly associated with the event was of less than 40 dBZ intensity. The only exception was a small area of embedded 45 dBZ returns with echo tops from 28-33 Kft that developed along the aircraft's approach path near the time of the incident (Figure 6).

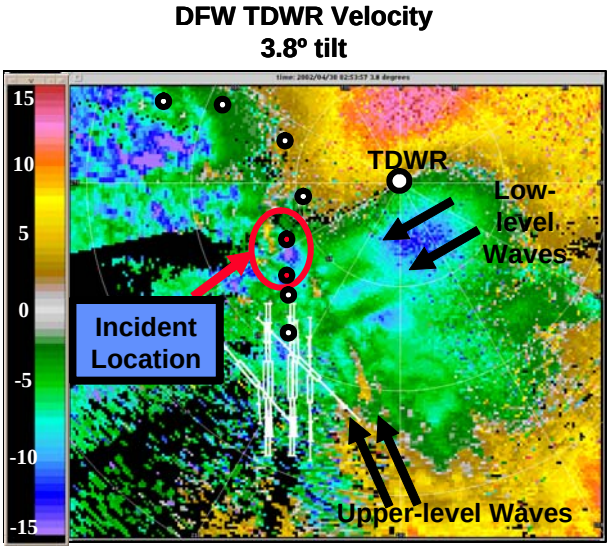

Figure 5. A Doppler velocity image from the DFW TDWR at the time of the intersecting buoyancy waves encounter on 30 April 2002. The arrows illustrate the locations of the two sets of BW waves. Dots represent the flight path of the MD-80 and the red dots denote the location where the aircraft encountered the severe turbulence. Scale shown in units of m/s.

The incident occurred in the vicinity of a strong wind shift boundary associated with a line of precipitation. This boundary was more pronounced near the altitude of the aircraft turbulence encounter (between 1000 – 2000 ft) than near the surface. Alternating regions of negative and positive shear associated with the buoyancy waves (Figure 7) were evident in the Doppler radar returns. These waves combined with the rapid transition from headwind to tail winds appear to have caused the fluctuations in altitude and airspeed as the aircraft attempted its approach.

4. DETECTION APPROACHES

4.1 Radar image processing algorithms

Radar-based algorithms have shown considerable skill in detecting wind shear events associated with microbursts and gust fronts. An excellent example of this can be seen in the performance of the Integrated Terminal Weather System (ITWS) wind shear detection algorithms that have a demonstrated Probability of Detection (POD) for microburst events that exceeds 95%. The success of these algorithms is based on image processing techniques that are applied to the radar base data to extract the signatures associated with the phenomena.

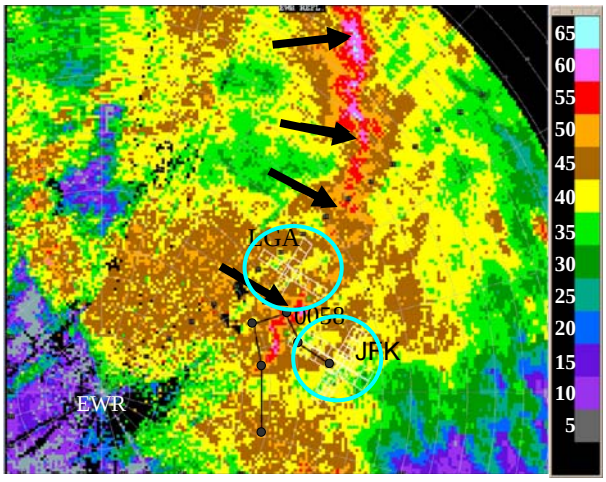

Figure 6. 0.3° tilt radar reflectivity returns (dBZ) from the Newark NJ (EWR) TDWR on 29 April 2002. The circles around the white rectangles denote the JFK and LGA Areas Noted for Attention (ARENAs). The black arrows show that the arc of embedded convection is co-located with the shear/wind shift boundary, which is shown in the next figure. The solid black line segments show the aircraft's approach path to Runway 13L at one-minute intervals (from Isaminger et al. 2003).

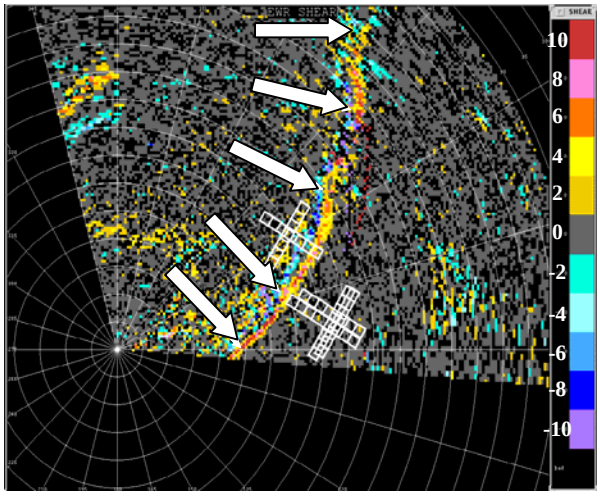

Figure 7. Radial velocity shear map from the 1.0° elevation tilt of the EWR TDWR. The shear boundary between LGA and JFK is clearly evident by the arc of positive shear (warm colors), denoted with the white arrows (from Isaminger et al. 2003).

Many of the documented buoyancy waves also exhibit a unique radar signature, making detection of these phenomena possible. The ITWS Machine Intelligent Gust Front Algorithm (MIGFA) uses a series of feature detectors to identify gust fronts in radar base data. The feature detectors look for signatures common to gust fronts, such as radial velocity convergence, and reflectivity thin lines. Evidence maps are then generated based on the existence of these features, and a gust front detection is made in regions where the evidence is greater than a predefined threshold. Figure 8 shows an image of the TDWR radial velocity from a DFW case with corresponding evidence maps called interest images. Notice that when velocity convergence due to the BW (the wave like pattern in the TDWR data) is present in the base data, the gust front interest values are higher. A modified version of the operational MIGFA algorithm could examine the radar data for the alternating convergence and divergence line signature associated with the buoyancy waves.

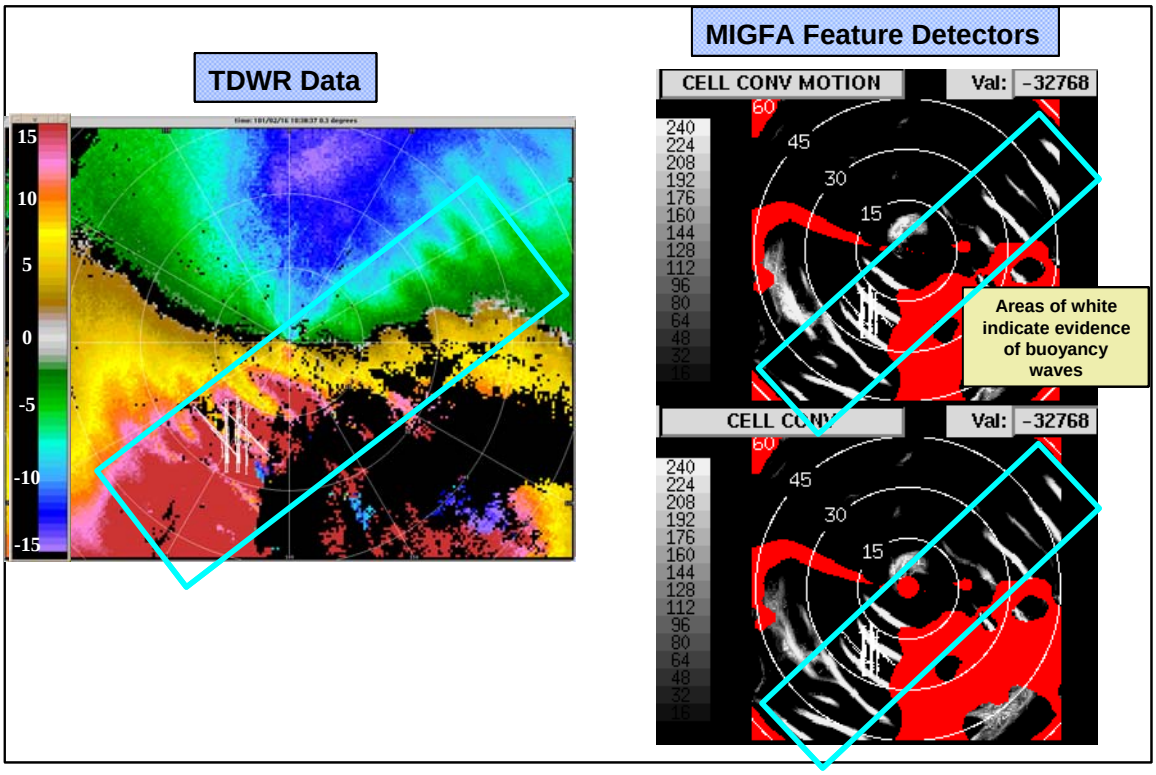

Figure 8. An example illustrating TDWR base data being used in a MIGFA based BW detection system. The Doppler radar velocity (in m/s) shown on the right are utilized by image processing tools to extract evidence of BW. The white areas in the MIGFA feature detectors indicate evidence of buoyancy waves.

This example illustrates that radar image processing based techniques could be employed to detect buoyancy waves. In contrast to current gust front signatures detected by MIGFA, the BW detection algorithm would need to examine more than the two near-surface radar tilts, given that buoyancy waves also exist at higher altitudes. This algorithm would also need to incorporate vertical profiles of temperature and winds that could pre-sensitize the algorithm during conditions conducive to BW development. The existence of the stability and vertical wind shear information features could increase the confidence that the radar image based evidence in fact represents a buoyancy wave, and reduce potential false alarm rates. Turbulence intensity could be estimated by the strength of the shear coincident with the buoyancy waves, and alerts would be generated if the value was greater than a specified threshold.

4.2 Path-based shear detection

A complementary if not alternative detection strategy is to compute a gridded wind analysis from the observations and combine this with knowledge of the anticipated aircraft flight path. This technique will work best with BW turbulence on scales $\geq$ 2 km.

Figure 9 illustrates the 4-D trajectory data for a five minute time span encompassing the uncontrolled descent of Boeing 767 from the 29 April 2002 incident at JFK. Figure 9a shows a time height plot of the trajectory data with the route heading indicated above the curve at each one-minute time step. The uncontrolled descent occurred from two to four minutes into the flight track plot. Figure 9b shows the geographic location of the trajectory with respect to JFK International Airport; arrows along the trajectory indicate the heading vector at each point. The largest wind shift occurred just as the aircraft was turning onto its final approach.

Given the 4-D trajectory of Boeing 767, one can interpolate the gridded horizontal wind information ($V_{2\text{-}D}$) provided by the ITWS Terminal Winds (Twinds) product (Cole and Wilson, 1994) to points along the trajectory. This is achievable first through linear interpolation of gridded values in the horizontal at each layer of the analysis, then through interpolation of the layered information in the vertical via the use of a cubic spline. The Twinds analysis for this exercise has a resolution of 1 km on a 121x121 km grid in the horizontal, with a 25 mb resolution in the vertical, and five minute temporal resolution. The nearest wind analysis that does not exceed the trajectory time is used for the path-based shear calculation.

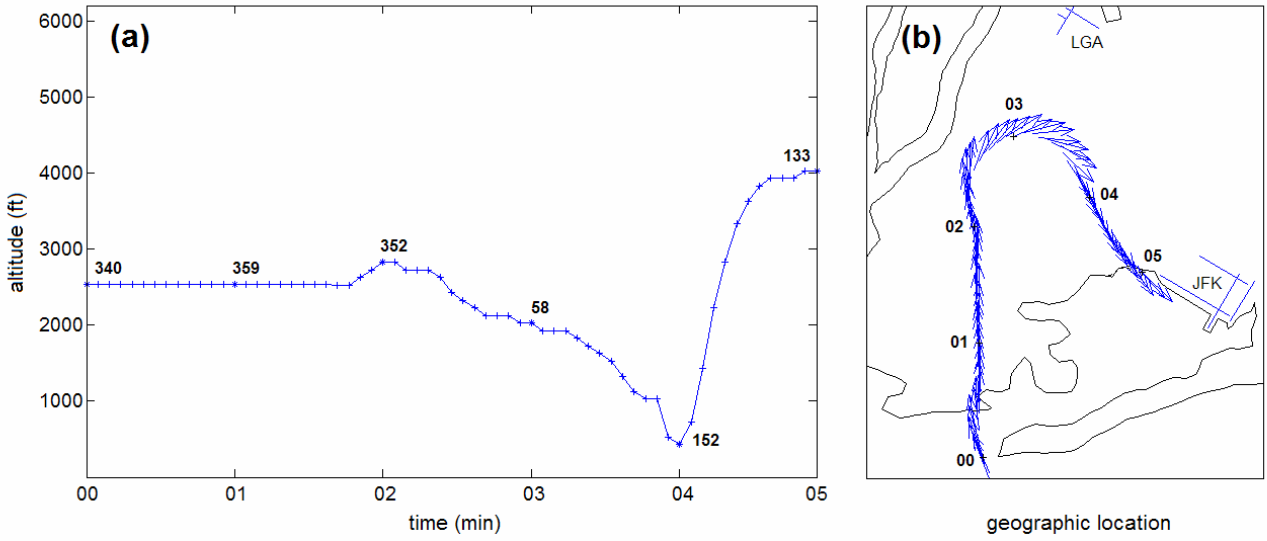

Figure 9. (a) Time-height plot of AAL16 trajectory from 0055Z to 01000 29 April 2002. Aircraft heading in degrees displayed above curve at 1 minute intervals. (b) Geographic location of AAL16 with respect to JFK. Blue vectors indicate heading at each trajectory point; the 1 minute interval is marked for reference with (a).

Heading information from the aircraft trajectory expressed as a 2-D unit vector ($\hat{h}$) is combined with $V_{2\text{-}D}$ at each point to determine headwind/tailwind. The headwind/tailwind is calculated as the dot product between $V_{2\text{-}D}$ and $\hat{h}$.

$$\text{Headwind/Tailwind} = -\left(V_{2\text{-}D} \cdot \hat{h}\right)$$

Positive quantities indicate a calculated headwind at each point along the trajectory; negative quantities indicate a calculated tailwind. These quantities are then combined along the full path length to produce the trajectory's headwind profile. This result is then smoothed with an iterative 5-point centered sliding window to remove small, jagged artifacts in the headwind profile. The smoothed headwind profile is then used to determine segments of anticipated airspeed loss or gain along the aircraft trajectory.

Given the aircraft's headwind profile, the point calculations of headwind/tailwind are examined iteratively to find local minima and maxima in the profile. Excluded from the search are local min/max pairs that do not exceed a ±2 kt difference between pairs. Those excluded min/max values are considered noise because those differences fall below the resolution error of the Twinds analysis and other errors attributable to heading calculations. For this case, if the difference between a retained min-max pair exceeds a loss or gain of ±10kts, the segment is deemed significant.

Figure 10 is a graphical representation of these significant path-based shear segments that corresponds to the times and planar positions seen in Figure 9a and Figure 9b respectively. The Boeing 767 headwind profile of Figure 10a shows the oscillatory change in headwind/tailwind experienced by the aircraft as it intersected the shear boundary and trailing buoyancy oscillations (Figure 7). Losses that exceed the -10 kt threshold are indicated in red; gains greater than 10 kt are indicated in blue. Throughout the time segment, losses/gains exceeded the set ±10 kt threshold five times in five minutes. The largest change, a 28 kt loss occurring between the two and four minute time markers, is the initial loss that contributed to incident.

This technique is used in a prototype Path-based Shear Detection (PSD) algorithm currently under development. The PSD algorithm is being developed in response to a need for an air traffic control support tool that addresses issues that arise during high wind and turbulent wind events. The PSD system will ingest data from the operational ITWS Twinds and concentrate that data into path-specific shear detection information. A web-based Java display will display the arrival paths of interest and highlight the segments along those paths where excessive gains and losses have been deemed significant. Figure 11 is an example of an experimental PSD display for New York airspace. For reference and an operational overview of the PSD algorithm and display, see Allan et al. (2004)

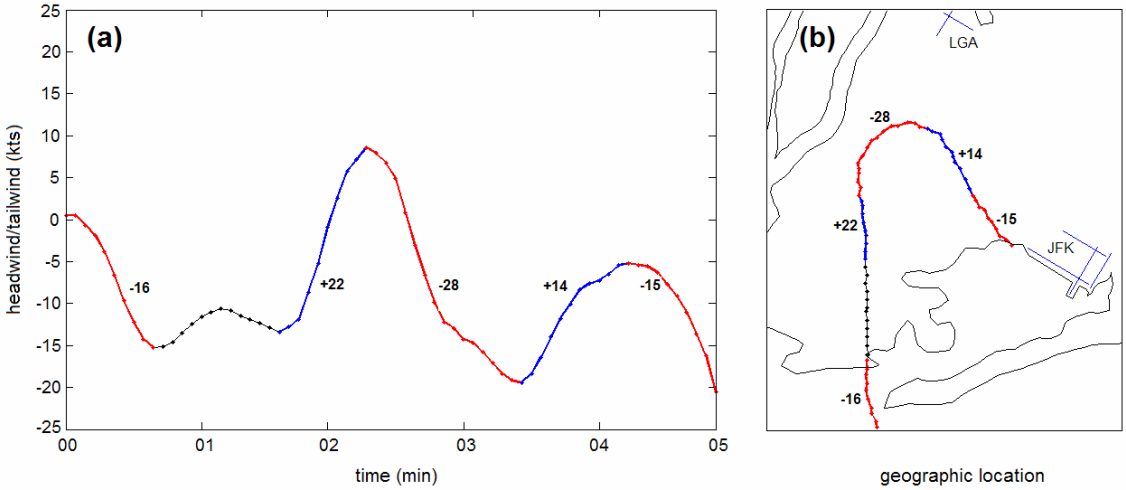

Figure 10. (a) Headwind profile of Boeing 767 on April 29, 2002. The ordinate axis indicates headwind/tailwind (kts) as positive/negative values respectively. Segments plotted in red indicate calculated potential aircraft airspeed losses exceeding -10kts; gains greater than 10 kts are plotted in blue. Calculated values at each loss/gain segment (kts) are labeled next to the curve. (b) Planar view showing geographic location of loss/gain segments for reference to Figure 10b.

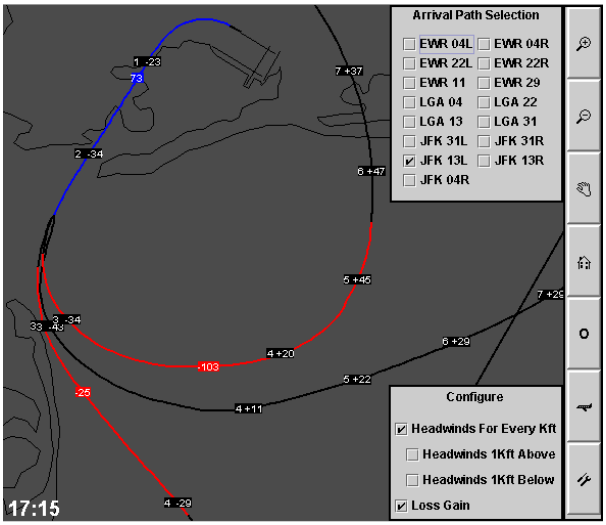

Figure 11. Display of PSD Tool with approach paths into JFK on runway 13L displayed. Arrival path segments where significant loss in headwinds is expected are colored in red. Arrival path segments where significant gain in headwind is expected are colored in blue. See Allan et al. (2004) for more details.

5. CONCLUSIONS

Aviation safety has been the beneficiary of significant advancements in the understanding of mesoscale wind shear phenomena. The discovery and research into microburst and gust front wind shear led to the development of wind shear detection and warning systems that have made air travel safer. It appears, however, that low altitude turbulence may also be a significant hazard to aviation.

The turbulence encounter statistics presented in this study indicate that a significant portion of the moderate or greater turbulence occurs below 18,000 feet. The recent incidents of low altitude turbulence encounters presented here provide clear evidence that they can be as dangerous as an encounter with microburst wind shear. While current wind shear detection systems are not designed to detect and warn for this phenomenon, the similarities between wind shear and BW turbulence make it feasible to modify existing wind shear detection systems to provide BW diagnosis and hazard detection. The radar and path-based shear detection techniques presented in this paper are examples of such modifications.

6. REFERENCES

Allan, S., R. DeLaura, B. Martin, D. Clark, C. Gross, and E. Mann, "Advanced Terminal Weather Products Demonstration in New York", *The American Meteorological Society*, this issue.

Bieringer, P. E. 2002: An overview of low altitude buoyancy wave induced turbulence impacts on commercial and civilian aviation. Preprints, 10th Conference on Aviation, Range, and Aerospace Meteorology, Portland, OR, *Amer. Meteor. Soc.*

Cole, R. E. and F. W. Wilson, "The Integrated Terminal Weather System Terminal Winds Product", *The Lincoln Laboratory Journal*, Fall 1994, Vol. 7, No 2.

Droegemeier, K. K. and R. Wilhelmson, 1987: Numerical simulation of thunderstorm outflow dynamics. Part 1: Outflow sensitivity experiments and turbulence dynamics. *J. Atmos. Sci.,* **44**, 1180-1210.

Isaminger M., Beesley, T. and B. Martin, "An Analysis of a Wind Shear Encounter at the John F. Kennedy International Airport (JFK) on 28/29 April 2002" Lincoln Laboratory Project Memorandum No. 43PM Wx-0089, 6 February 2003.

Miller, D. W., B. Boorman, R. Ferris, and T. Rotz, 1997: Characteristics of Thunderstorm Induced Gravity Waves Using Doppler Radar and Tower Instrumentation. Preprints, 28th Conference on Radar Meteorology, Austin, TX, *Amer. Meteor. Soc*., 165-167.

Miller, D. W., 1999: Thunderstorm Inducted gravity waves as a potential hazard to commercial aircraft. Preprints, 8th Conference on Aviation, Range, and Aerospace Meteorology, Dallas, TX, *Amer. Meteor. Soc.*

Meuse, C., L. Galusha, M. Isaminger, M. Moore, D. Rhoda, F. Robasky, and M. Wolfson, 1996: Analysis of the 12 April wind shear incident at DFW airport, 1996 Workshop on Wind Shear and Wind Shear Alert Systems, Oklahoma City, OK *Amer. Meteor. Soc*., 23-33.

Proseus, E.A. and B.D. Martin, "The Crash of FedEx Flight 674: Analysis of TDWR and Terminal Winds Data", Lincoln Laboratory Project Memorandum No. 43-7260, 20 February 2004.

Simpson, J. E., 1969: A comparison between laboratory and atmospheric density currents. *Quart. J. Roy. Meteor. Soc*., **95**, 758-765.

Xu, Qin, Xue, Ming, Droegemeer, Kelvin K. 1996: Numerical Simulations of Density Currents In Sheared Environments within a Vertically Confined Channel. *Journal of the Atmospheric Sciences*: **53**, pp. 770–786.